Colloid Polym Sci (2005) 283: 1070–1078
DOI 10.1007/s00396-004-1237-6

Keita Suzuki
Jun-ichi Oku
Kenichi Izawa
Hiro-Fumi Okabayashi
Isao Noda
Charmian J. O'Connor

Two-dimensional gel permeation chromatography (2-D GPC) correlation studies of the aggregate–aggregate interactions in acid-catalyzed triethoxysilyl-terminated polystyrene systems: weak catalysis by HNO_3

Received: 9 July 2004
Accepted: 15 October 2004
Published online: 4 May 2005

K. Suzuki · J. Oku
H.-F. Okabayashi (✉)
Department of Applied Chemistry,
Nagoya Institute of Technology,
Gokiso-cho, Showa-ku, Nagoya,
Aichi 466-8555, Japan
E-mail: fwiw4348@mb.infoweb.ne.jp

K. Izawa
Chromato Department,
Fuji Silysia Chemical Ltd., 1846, Kozoji2,
Kasugai, Aichi 487-0013, Japan

I. Noda
The Procter and Gamble Company, 8611
Beckett Road, West Chester, 45069, OH,
USA

C. J. O'Connor
Department of Chemistry, The University
of Auckland, Private Bag 92019, Auckland,
New Zealand

Abstract Time-resolved gel-permeation chromatography (GPC) profiles were measured over a long period of time ($t = 0$–768 h) for the HNO_3-catalyzed reaction mixture of a well-defined polymeric silane coupling agent, triethoxysilyl-terminated polystyrene. The results showed that HNO_3 catalyzes the rate of polymerization, but only to a small extent. Two-dimensional (2-D) GPC correlation spectra were calculated from time-resolved GPC profiles and were used to examine the mechanism of polymerization. The resolution enhancement obtained by 2-D correlation provided ample evidence for existence of four monomeric components. It has been demonstrated that dynamic variation in the population of these components occurs over a long reaction time, reflecting the mechanism of a slow polymerization process.

Keywords 2-D GPC correlation · Triethoxysilyl-terminated polystyrene · Slow-reactivity · HNO_3-catalyst

Introduction

Silane coupling agents (SCA) are commonly used to reinforce the mechanical properties of the interface between two different materials. Extensive studies have been carried out on their macroscopic properties [1–3] and molecular structure [4–19] when they are coated onto the surface of a substrate. One of the most commonly used SCAs, which provide hydrophobic character to a surface, is alkyltriethoxysilane (ATES). In the acid-catalyzed ATES system, an acid catalyst induces hydrolysis of the ethoxy groups to produce silanol groups. The silanol groups react to form a siloxane linkage between two silane molecules, with the release of ethanol and formation of another H_2O molecule (reactions I and II).

$$RSiL_2(OC_2H_5) + H_2O \xrightarrow[\text{catalyst}]{} RSiL_2(OH) + C_2H_5OH \quad \text{(I)}$$

$$2RSiL_2(OH) \rightarrow RSiL_2 - O - SiL_2R + H_2O \quad \text{(II)}$$

R = alkyl group, $L = -OC_2H_5$, $-OH$ or $-O-Si$

Izawa et al. [20–22] used time-resolved gel permeation chromatography (GPC) profiles and two-dimensional (2-D) GPC correlation spectra to examine the reaction

mechanism in the relatively simple ATES-ethanol systems catalyzed by 1.0 M $HCl{\cdot}H_2O$. The results showed that polymeric precursors are formed not only by fully hydrolyzed monomers but also by partially hydrolyzed species. The weak intensities of the elution bands of the monomeric species in the GPC profiles hindered the elucidation of their critical role in the overall mechanism of the growth process. However, resolution enhancement of the 2-D GPC correlation spectrum [20–22] made it possible to discuss in detail the significant role that the monomer played.

The time-resolved GPC profiles for the CH_3SO_3H- or HCl-catalyzed reaction mixture of a macromolecular SCA, triethoxysilyl-terminated polystyrenes (TESi-PS) [23, 24], furnished only the elution band of unhydrolyzed TESi-PS. Elution bands which might be assigned to fully or partially hydrolyzed monomers were not observed. The resolution enhancing character of 2-D GPC correlation maps is useful for predicting the existence of these hydrolyzed monomeric species. In fact, only one elution band coming from partially or fully hydrolyzed monomeric species is predicted, and this will have a higher elution count than that of the unhydrolyzed TESi-PS monomer [23, 24]. However, its assignment still remains equivocal. Therefore, identification of the elution bands of mono-, di- and tri-hydroxyalkylsilane becomes critical for elucidation of the polymerization mechanism.

In the present study, 2-D GPC correlation spectra are used to examine details of the polymerization process in the HNO_3-catalyzed TESi-PS system. In particular, the correlation of unhydrolyzed TESi-PS and its hydrolyzed species with polymeric precursors is discussed with respect to the mechanism of slow polymerization.

Experimental

Materials

Living polystyrene (PS) with molecular weight (Mn) equal to 7,800 was synthesized by anionic polymerization of styrene [25]. TESi-PS with Mn equal to 8,000 was prepared by the coupling reaction of living PS and chlorotriethoxysilane [25]. The sample (TESi-PS), which was reprecipitated in methanol, was used for condensation after drying in vacuum at ca. 298 K. Samples of the reaction systems (TESi-PS (40 mmol/kg), catalyst (HNO_3, 0.1 mol/kg) and tetrahydrofuran (THF)) were placed into each ampoule, and sealed under high vacuum (10^{-3} mm Hg). Condensation of TESi-PS in each reaction mixture was carried out in a temperature-controlled bath (333 K) for a prescribed time. The condensed products of TESi-PS, precipitated from each reaction mixture, were filtered through a glass filter and dried at ca. 298 K.

The yield (Y (%)) of polymerized TESi-PS was calculated from the GPC curve of the recovered polymer using the equation

$$Y(\%) = \frac{\text{GPC peak area of polymerized TESi} - \text{PS}}{\text{Total GPC peak area of the reaction products}} \times 100.$$

The functionality of TESi-PS (f (%): the maximum Y value of TESi-PS) was 98%. The contribution of the band for the unfunctionalized trace constituent, which was obtained from control experiments of the sample system, to the band for the total condensed product was 2%. This contribution was subtracted from the area of polymerized TESi-PS to obtain the value of Y.

The area of polymerized TESi-PS was calculated from that of GPC peak detected by the difference in refractive index (RI) between the peak component and the solvent THF. It was confirmed that the peak area obtained by the RI difference was equal to that determined simultaneously from the difference in UV (360 nm)-absorbance.

Time-resolved GPC measurements

A Toso HLC-802A (with two GMH columns), equipped with RI and UV detectors (column oven temperature 313 K), was used for the GPC measurements. THF was used as the eluent at the nominal flow rate of 1 mL/min. The actual flow rate was inspected during the recording of a GPC curve, and its constancy was confirmed (the errors of an elution count: ± 0.1 min and the average signal-to-noise ratio of the GPC data: less than 170). The amount of TESi-PS-catalyst-THF solution injected into the GPC column was controlled to provide a linearly increasing RI and a linearly increasing UV absorbance (at 360 nm).

A GPC calibration curve with linear PS standards, whose application to the branched products of TESi-PS had already been confirmed [26], was used to make assignments.

Two-dimensional gel permeation chromatography correlation analysis

Synchronous and asynchronous 2-D GPC correlation spectra were calculated from the time-resolved GPC profiles, using the 2-D OGAIZA software developed at Nagoya Institute of Technology. The theoretical background of 2-D GPC spectra has been described in recent publications [20–22, 27].

Results and discussion

Time-resolved GPC profiles

Time-resolved GPC profiles of the HNO_3-catalyzed TESi-PS-THF system, which provide the time-dependence of the composition in this reaction mixture, are shown in Fig. 1. Assignments of the elution bands are listed in Table 1 together with those based on the 2-D GPC correlation spectra.

The elution bands A, B and shoulder C correspond to monomer, dimer and trimer, respectively. With time, the intensity of band A decreases, while that of bands B and C increases, reflecting the fact that consumption of the TESi-PS monomers occurs to produce the dimers and trimers.

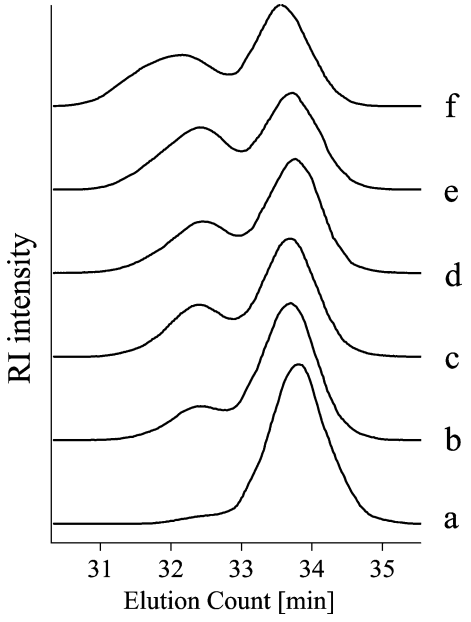

Fig. 1 Time-resolved GPC profiles of the 0.1 mol/kg HNO_3-catalyzed TESi-PS-THF systems (reaction time (t), *a*: $t = 0$ h, *b*: $t = 4$ h, *c*: $t = 16$ h, *d*: $t = 24$ h, *e*: $t = 144$ h, *f*: $t = 768$ h)

Figure 2 shows the time courses of the yield Y (%), and of the percentage (Z (%) = 100 − Y (%)) of the monomers remaining unreacted. It is found that the yield increases logarithmically until it finally approaches 43% at 144 h and then remains almost constant. We note that band A, for the TESi-PS monomers remaining unreacted, is predominant even in the GPC profile obtained at 768 h.

In comparison, the corresponding Y values of condensed products, obtained at 24-h reaction time in the CH_3SO_3H- and HCl-catalyzed TESi-PS-THF systems [23, 24], are 95 and 93%, respectively. Therefore, it is evident that the yield (43%) in the HNO_3-catalyzed system is very low.

We calculated the rate constant of this condensation reaction from the Z values, assuming that the time course of Z can be expressed by $Z = A \exp(-kt) + B$, where k (s^{-1}) is the rate constant of the reaction. The rate constant, obtained from the best fit between the observed and calculated Z values, is $k = 6.64 \times 10^{-5}$ s^{-1}, an order of magnitude smaller than those ($k = 7.25 \times 10^{-4}$ s^{-1} and $k = 4.66 \times 10^{-4}$ s^{-1}) obtained for the CH_3SO_3H− [28] or HCl-catalyzed TESi-PS-THF systems, respectively.

In our previous study [29] we have already reported that the condensation reaction did not occur in the TESi-PS-THF solution in the absence of catalysts, even after heating at 333 K for 72 h. Therefore, although HNO_3 catalyzes the condensation of TESi-PS molecules, its ability to do so is much less than that of the acid catalysts, such as HCl and CH_3SO_3H.

In this study, we used 2-D GPC correlation analysis to examine the detailed mechanism for this slow polymerization.

Two-dimensional correlation GPC spectra

In the synchronous spectrum for step I (0–24 h) for the HNO_3-catalyzed TESi-PS-THF system (Fig. 3a), very strong fused autopeaks consisting of two autopeaks are

Table 1 Tentative assignment of elution peaks

Conventional GPC		2-D GPC		Assignment
Counts (min)	Band no.	Counts (min)	Band no.	
		34.4	$A_{H'}$	THSi-PS (trihydrolyzed monomer)
		34.0–34.2	A_H	THSi-PS (dihydrolyzed monomer)
33.8	A	33.6–33.9	A	TESi-PS (monomer and monohydrolyzed monomer)
		33.3–33.5	A_L	Solvated monomer
32.5	B	32.5–32.6	B	Dimer
		32.4–32.2	B_L	
31.6	C	31.6–31.8	C	Trimer
		31.2–31.4	C_L	
31.0	D	31.0–31.1	D	Tetramer

The errors of elution peaks are ±0.1 min
Subscript H high elution component, *subscript L* low elution component

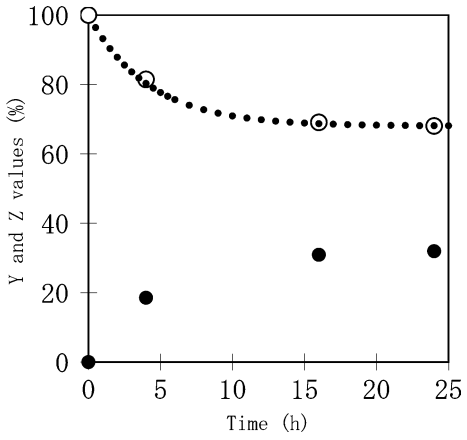

Fig. 2 Time courses of *Y* (*filled circle*) and *Z* (*open circle*) (*broken line*: the calculated best fit curve)

observed at 33.9 and 34.2 min, which arise from components A and A_H, respectively. Since the contour levels of these autopeaks are extended in the region $E_1 = E_2 = 33.2$–34.8 min, we may expect that the autopeaks arising from lower and higher elution bands (A_L and $A_{H'}$) are further superimposed with the autopeaks of A or A_H. The other strong autopeak at 32.4 min is ascribed to component B_L. The positive cross peaks at (34.2, 33.9) and (33.9, 34.2) min arise from the $A \leftrightarrow A_H$ correlation. The negative cross peaks consisting of the two fused negative peaks at (34.2, 32.4) and (33.9, 32.4) min, or at (32.4, 34.2) and (32.4, 33.9) min, arise from the $A_H \leftrightarrow B_L$ and $A \leftrightarrow B_L$ correlations, respectively. These autopeaks and cross peaks together define the correlation squares CSq_1, CSq_2 and CSq_3 (Table 2) [27]. Since the intensities of these correlation peaks are very strong, the $A \leftrightarrow A_H$, $A_H \leftrightarrow B_L$ and $A \leftrightarrow B_L$ correlations are the dominant contributors to step I.

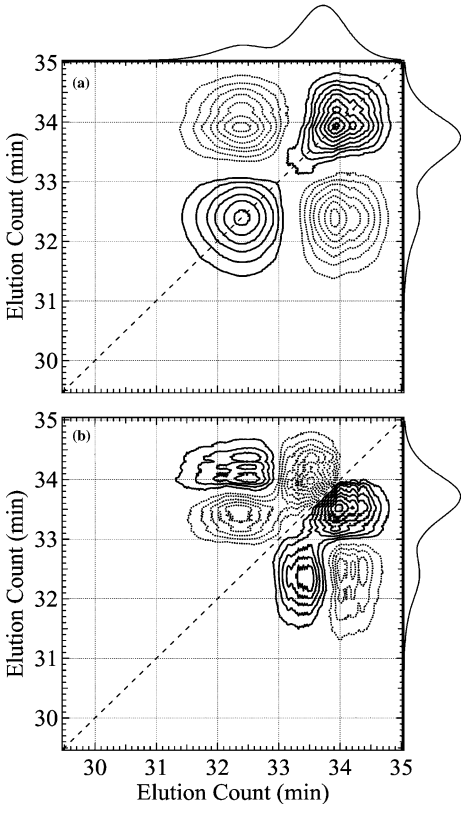

Fig. 3 Synchronous (**a**) and asynchronous (**b**) spectra of step I (0, 4, 16 and 24 h) for the HNO_3-catalyzed TESi-PS-THF systems

As a consequence of resolution enhancement [24], we now see in the asynchronous spectrum (step I) for the same system (Fig. 3b and Table 3) that the positive cross peaks in the region $E_1 = 33.5$–34.8, $E_2 = 33.0$–34.0 min consist of the three fused cross peaks at (34.0, 33.5), (34.2, 33.5) and (34.4, 33.5) min. These cross peaks arise from asynchronous correlations $A \leftrightarrow A_L$, $A_H \leftrightarrow A_L$ and $A_{H'} \leftrightarrow A_L$, reflecting that different dynamic variations of the monomeric components (A_L, A, A_H and $A_{H'}$) occur in step I. We find that extension of the positive cross peak in the region $E_1 = 33.0$–33.8, $E_2 = 31.5$–33.0 min, in which the A_L component asynchronously correlates with components B_H, B, B_L and C, indicating that consumption of A_L to produce the B and C components, may not occur in a single isolated step. Furthermore, the negative fused cross peaks extend in the region $E_1 = 33.8$–34.7, $E_2 = 31.5$–33.0 min. Therefore, components A, A_H and $A_{H'}$ correlate with the dimeric and trimeric components B_L, B and C. From the relative intensities of two of the positive and one of the negative fused cross peaks, it is evident that three monomeric hydrolyzed components are produced predominantly in step I, and a significant amount of the unreacted monomer still remains.

In our previous studies [23, 24], we confirmed, after carrying out resolution enhancement, that splitting of band A occurs to provide components A and A_H. The two components were tentatively assigned to TESi-PS and its mono-hydrolyzed species and to the di- and trihydrolyzed monomers, respectively. However, the existence of component $A_{H'}$ was not confirmed. In this study, we have confirmed, for the first time, the existence of component $A_{H'}$, thereby making it possible to assign the trihydroxy species.

The synchronous map for step II (24–768 h), of the same sample system, is shown in Fig. 4a. The strong autopeak at 34.0 min, the two very weak autopeaks at 33.4 and 32.6 min and the weak autopeak at 31.6 min are assigned to components A, A_L, B and C, respectively. The very weak positive cross peaks at (34.0, 32.6), (32.6, 34.0), (33.3, 31.6) and (31.6, 33.3) min are assigned to the $A \leftrightarrow B$ and $A_L \leftrightarrow C$ correlations. The relatively strong negative cross peaks at (34.0, 31.6) and (31.6, 34.0) min, the very weak cross peaks at (34.0, 33.3), (33.3, 34.0), (33.4, 32.6), (32.6, 33.4), (32.6, 31.5) and

Table 2 Possible correlation squares (CSq_i) and correlations between the elution peaks in steps I and II

CSq_i	Coordinates (E_1, E_2)				Correlation
	Autopeak		Cross-peak		
Step I (0–24 h)					
CSq_1	+(34.2, 34.2)	+(33.9, 33.9)	+(34.2, 33.9)	+(33.9, 34.2)	$A \leftrightarrow A_H$
CSq_2	+(34.2, 34.2)	+(32.4, 32.4)	−(34.2, 32.4)	−(32.4, 34.2)	$A_H \leftrightarrow B$
CSq_3	+(33.9, 33.9)	+(32.4, 32.4)	−(33.9, 32.4)	−(32.4, 33.9)	$A \leftrightarrow B$
Step II (24–768 h)					
CSq_1	+(33.9, 33.9)	+(33.4, 33.4)	−(33.9, 33.4)	−(33.9, 33.9)	$A \leftrightarrow A_L$
CSq_2	+(33.9, 33.9)	+(32.6, 32.6)	+(33.9, 32.6)	+(32.6, 33.9)	$A \leftrightarrow B$
CSq_3	+(33.9, 33.9)	+(31.6, 31.6)	−(33.9, 31.6)	−(31.6, 33.9)	$A \leftrightarrow C$
CSq_4	+(33.4, 33.4)	+(32.6, 32.6)	−(33.4, 32.6)	−(32.6, 33.4)	$A_L \leftrightarrow B$
CSq_5	+(33.4, 33.4)	+(31.6, 31.6)	+(33.4, 31.6)	+(31.6, 33.4)	$A_L \leftrightarrow C$
CSq_6	+(32.6, 32.6)	+(31.6, 31.6)	−(32.6, 31.6)	−(31.6, 32.6)	$B \leftrightarrow C$

(31.5, 32.6) min arise, respectively, from correlations $A \leftrightarrow C$, $A \leftrightarrow A_L$, $A_L \leftrightarrow B$ and $B \leftrightarrow C$.

The four autopeaks and twelve cross peaks provide six correlation squares CSq_i ($i = 1$–6) (Table 2) [26]. CSq_1 implies that component A is consumed to form component A_L and that a coordinated decrease in intensity of component A and simultaneous increase in intensity of component A_L occur. CSq_i ($i = 1$–3) include the strong autopeaks at 33.9–34.0 min in common, reflecting that dynamic variation in the population of component A is a major contribution to step II. For the other correlation squares CSq_i ($i = 4$–6), each square reflects a similar coherent variation in component intensity. However, their contributions to step II must be small, since their relative intensities are very weak.

In the asynchronous map (step II) of the same system (Fig. 4b and Table 3), we see a very strong negative fused cross peak at (33.9, 33.4), which indicates the existence of separate components A_L and A. The sign of this coordinate at (33.9, 33.4) is negative in both the synchronous and asynchronous maps. Therefore, the decrease in intensity of component A occurs before that of component A_L. Furthermore, the relatively strong negative cross peak at (34.2, 33.9) provides evidence for the existence of components A and A_H in step II.

For the very strong positive cross peak arising from the $A \leftrightarrow B$ correlation, signs and order of events (Table 3) indicate that component A decreases in intensity before component B. (In other words, the consumption of A does not result directly in the production of B, as these events do not happen simultaneously, but involve some intermediates and side products.) The synchronous cross peak, on the other hand, is a good indicator that overall reduction of A leads to the production of B.

The negative $A \leftrightarrow C_L$ and positive $B \leftrightarrow C$ correlation peaks reflect the consumption of the monomeric and dimeric species to produce the trimeric species (C and C_L). The presence of these asynchronous peaks indicates

Table 3 Synchronous and asynchronous peak correlations, signs and order of events for the HNO_3-catalyzed systems

Step	Correlation	Sign		Order of events[a]
		Synchronous (Φ)	Asynchronous (Ψ)	
I	$A_H \leftrightarrow A$ (s)	+	−	$A \rightarrow A_H$
	$A_{H'}, A_H \leftrightarrow A_L$ (s)	+	+	$A_{H'}, A_H \rightarrow A_L$
	$A \leftrightarrow A_L$ (vs)	+	+	$A \rightarrow A_L$
	$A_{H'} \leftrightarrow B$ (m)	−	−	$A_{H'} \rightarrow B$
	$A_H, A \leftrightarrow B$ (m)	−	−	$A_H, A \rightarrow B$
	$A_{H'} \leftrightarrow B_L$ (w)	−	−	$A_{H'} \rightarrow B_L$
	$A, A_H \leftrightarrow B_L$ (m)	−	−	$A, A_H \rightarrow B_L$
	$A_{H'}, A_H, A \leftrightarrow C$ (vw)	−	−	$A_{H'}, A_H, A \rightarrow C$
	$A_L \leftrightarrow B_L$ (s)	−	+	$B_L \rightarrow A_L$
II	$A_{H'} \leftrightarrow A$ (vw)	+	−	$A \rightarrow A_{H'}$
	$A_H \leftrightarrow A$ (w)	+	−	$A \rightarrow A_H$
	$A \leftrightarrow A_L$ (s)	−	−	$A \rightarrow A_L$
	$A \leftrightarrow B$ (vs)	+	+	$A \rightarrow B$
	$A \leftrightarrow C_L$ (m)	−	−	$A \rightarrow C_L$
	$A_L \leftrightarrow C$ (m)	+	−	$C \rightarrow A_L$
	$A_L \leftrightarrow B_L$ (vw)	−	+	$B_L \rightarrow A_L$
	$A \leftrightarrow D$ (vw)	−	−	$A \rightarrow D$
	$B \leftrightarrow C$ (m)	−	+	$C \rightarrow B$
	$B_H \leftrightarrow B_L$ (w)	+	+	$B_H \rightarrow B_L$

vs very strong, *s* strong, *m* medium, *w* weak, *Subscripts H and L* high and low elution components

[a] $E_x \rightarrow E_y$; the event E_x occurs before E_y

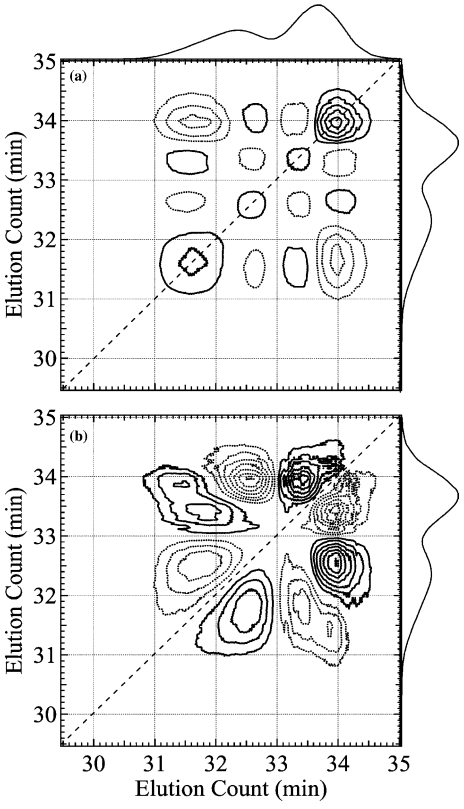

Fig. 4 Synchronous (**a**) and asynchronous (**b**) spectra of step II (24, 144 and 768 h) for the HNO_3-catalyzed TESi-PS-THF systems

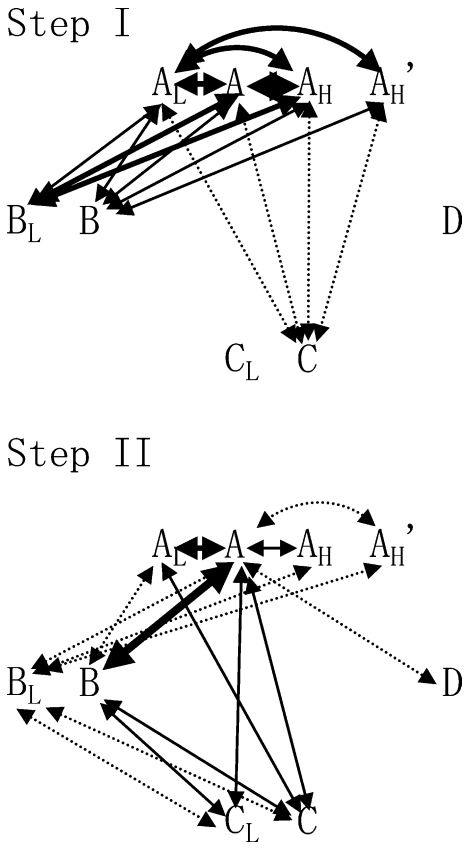

Scheme 1 Schematic growth process for HNO_3-catalyzed TESi-PS-THF systems

that the consumption of monomer is not directly coupled with the production of trimer (or dimer) in a single isolated step. It involves the formation of dimer and later trimer, with some other side steps like the formation of solvated species. Thus, there is no one-to-one relationship between the decrease in monomer and increase in trimer. Asynchronous peaks confirm the breakdown of a simplistic picture of reaction mechanism. However, the intensity of the A ↔ B correlation is more intense, compared with those of the other correlations (A, A_L ↔ C_L, C and B ↔ C). Thus, even in step II, dynamic variation in population of the A and B components is predominant.

We may now propose a model for the band correlations, which is consistent with the results suggested from the synchronous and asynchronous behaviors for steps I and II, as follows (Scheme 1). *Step I*: The correlations A ↔ A_H, A ↔ A_L, A_L ↔ A_H and A_L ↔ $A_{H'}$ and the correlations of these monomeric components with components B_L, B and B_H are very strong. Therefore, production of the three hydrolyzed monomeric components and consumption of A components to form the dimeric B components is predominant.*Step II*: The correlations of component A with components A_L and A_H are relatively strong. However, the A ↔ $A_{H'}$ correlation becomes very weak. A very strong A ↔ B correlation and the intermediate strength correlations A ↔ C_L, A_L ↔ C and B ↔ C (or C_L) still appear in this step. Therefore, the monomeric components A and A_L correlate with the dimeric and trimeric components over a long reaction time. This fact may indicate that these monomeric components effectively hinder progress of the condensation reaction. Furthermore, the correlations of C_L and C with longer oligomers, which would lead to further growth, do not appear, although we do see correlations between B_L and B with B_H ↔ C_L and C.

Conversely, in the CH_3SO_3H-catalyzed TESi-PS-THF-system [23], dynamic variation of the monomeric components to produce short oligomers is predominant in step I. However, it becomes very small in step II, following further growth of short oligomers.

Thus, it is evident that the reaction mechanism in this present HNO_3-catalyzed system is different from that in the CH_3SO_3H-catalyzed system [23].

However, additional independent supporting data should further strengthen the validity of this proposed model. In order to explain the behavior of the monomeric components in the HNO_3-catalyzed reaction process, we may use the experimental results for hydrolysis of condensed TESi-PS products, previously described

[28, 30], to postulate the existence of the cascade steps during the condensation reaction in steps I and II.

In step I

$$\mathrm{A} \underset{\leftarrow}{\rightarrow} \mathrm{A_L}, \mathrm{A_H}, \mathrm{A_{H'}} \tag{1}$$

$$\mathrm{A}, \mathrm{A_H}, \mathrm{A_{H'}} \rightleftarrows \mathrm{B_L}, \mathrm{B}, \mathrm{B_H} \tag{2}$$

$$\mathrm{A_L} \rightleftarrows \mathrm{B_L}, \mathrm{B}, \mathrm{B_H} \tag{3}$$

$$\mathrm{A_L}, \mathrm{A}, \mathrm{A_H}, \mathrm{A_{H'}} \underset{\leftarrow}{\rightarrow} \mathrm{C} \tag{4}$$

$$\left\{ \begin{array}{r} 3\mathrm{A}(\text{or } 3\mathrm{A_L} \text{or } 3\mathrm{A_H} \text{ or } 3\mathrm{A_{H'}}) \underset{\leftarrow}{\rightarrow} \mathrm{C} \\ \mathrm{A} \text{ (or } \mathrm{A_L} \text{or } \mathrm{A_H} \text{ or } \mathrm{A_{H'}}) + \mathrm{B}(\text{or } \mathrm{B_L} \text{ or } \mathrm{B_H}) \underset{\leftarrow}{\rightarrow} \mathrm{C} \end{array} \right\}$$

Cascade step (1) is predominant, reflecting the rapid production of three components (A_L, A_H and $A_{H'}$). The processes in steps (2) and (3) also occur to produce components B_L and B. The dimeric components thus produced are reversibly hydrolyzed to reform monomeric species in the HCl-catalyzed TESi-PS-THF-system. Therefore, the cascade steps (2) and (3) probably hinder the consumption of monomers. The contribution of cascade step (4) to step I may be small, since the correlations of these monomeric components with component C is weak (Fig. 4).

In step II, we may also propose the following cascade steps.

$$\mathrm{A} \underset{\leftarrow}{\rightarrow} \mathrm{A_L}, \mathrm{A_H}, \mathrm{A_{H'}} \tag{5}$$

$$\mathrm{A} \rightleftarrows \mathrm{B} \tag{6a}$$

$$\mathrm{A_L}, \mathrm{A}, \mathrm{A_H}, \mathrm{A_{H'}} \rightleftarrows \mathrm{B_L} \tag{6b}$$

$$\mathrm{A}, \mathrm{A_L} \underset{\leftarrow}{\rightarrow} \mathrm{C}, \mathrm{C_L} \tag{7}$$

$$\left\{ \begin{array}{r} 3\mathrm{A}(\text{or } 3\mathrm{A_L}) \underset{\leftarrow}{\rightarrow} \mathrm{C}, \mathrm{C_L} \\ \mathrm{A}(\text{or } \mathrm{A_L}) + \mathrm{B} \underset{\leftarrow}{\rightarrow} \mathrm{C}, \mathrm{C_L} \end{array} \right\}$$

$$\mathrm{B_L}, \mathrm{B}, \mathrm{B_H} \underset{\leftarrow}{\rightarrow} \mathrm{C}, \mathrm{C_L} \tag{8}$$

$$\left\{ \mathrm{B} \text{ (or } \mathrm{B_L} \text{ or } \mathrm{B_H}) + \mathrm{A}(\text{or } \mathrm{A_L}) \underset{\leftarrow}{\rightarrow} \mathrm{C}, \mathrm{C_L} \right\}$$

$$\mathrm{A} \underset{\leftarrow}{\rightarrow} \mathrm{D} \tag{9}$$

$$\left\{ \begin{array}{r} \mathrm{A} + \mathrm{C} \underset{\leftarrow}{\rightarrow} \mathrm{D} \\ 4\mathrm{A} \underset{\leftarrow}{\rightarrow} \mathrm{D} \end{array} \right\}$$

In the synchronous map (step II) (Fig. 4b), component A correlates in common with components A_L, B and C to construct CSq_1, CSq_2 and CSq_3. The intensity of the autopeak at 34.0 min arising from component A is the strongest, while those of the other three autopeaks (corresponding to components A_L, B and C) are weak or very weak. This difference in intensity among autopeaks indicates directly that dynamic variation in population of component A is more rapid than those of the other three components. Accordingly, cascade steps (6a) and (6b) may provide the very strong correlations A ↔ A_L and A ↔ B. The cascade step (8) may provide the correlations of the dimeric components (B_L, B and B_H) with components C_L and C, indicating that the trimeric components are produced as a consequence of reaction between B (or B_L) and A (or A_L).

Cascade steps (4) and (9) probably describe the contribution to the overall reaction of the self-assembled TESi-PS system [28] since an equilibrium ($n\mathrm{A} \rightleftarrows \mathrm{A}_n$) is possible between n moles of A and an aggregate of aggregation number equal to n, according to the mass-action law.

Furthermore, correlations of component C_L with longer oligomers do not appear in steps I or II, thereby implying that the C_L component is less-reactive and does not contribute to further growth [24].

Recently, we reported for the TESi-PS-THF system that the nature of the catalyst affects the growth process of polymerization [24, 25]. Reactive oligomers lead to further growth of polymeric precursors in the CH_3SO_3H-catalyzed system [25], while less-reactive oligomers hinder further growth of the oligomers in the HCl-catalyzed TESi-PS-THF-system [24].

In particular, the 2-D GPC results provided evidence that the reactive trimeric component C contributes to its further growth, while the less-reactive C_L component does not grow. For the mechanism of formation of the less-reactive species, we proposed the structural transfer model of the trimer. In this model, intramolecular condensation between the silanol groups in the monocyclic trimer occurs to form the bicyclic trimer with fewer silanol groups. This decrease in the number of SiOH groups results in reduction in reactivity of the trimer. However, this model is not applicable to the present HNO_3-catalyzed system.

In order to explain the slow progress of a condensation reaction in the HNO_3-catalyzed TESi-PS-THF system (molar ratio [HNO_3]:[SiOH] ≈ 1:1), we invoke the following hypothesis.

We assume a reversed micellar type TESi-PS aggregate with a polar core in THF [28]. Unhydrolyzed ethoxy groups, water and catalysts are concentrated in the core, and the interface is formed between the oil (THF-TESi-PS) and water phases (Fig. 5a).

A TESi-PS molecule has three Si–O–C segments partially charged (Si^{8+}–O^{8-}–C^{8+}) and a HNO_3 catalyst also provides a partially charged counter anion ($O=N^{8+}$ ($-O^{8-}$)$_3$). Therefore, the coordination of this counter anion to the Si–O–C segment makes it possible to form the Si–O–C···NO_3 complex (Fig. 5b), providing a relatively stable TESi-PS molecule. Formation of this

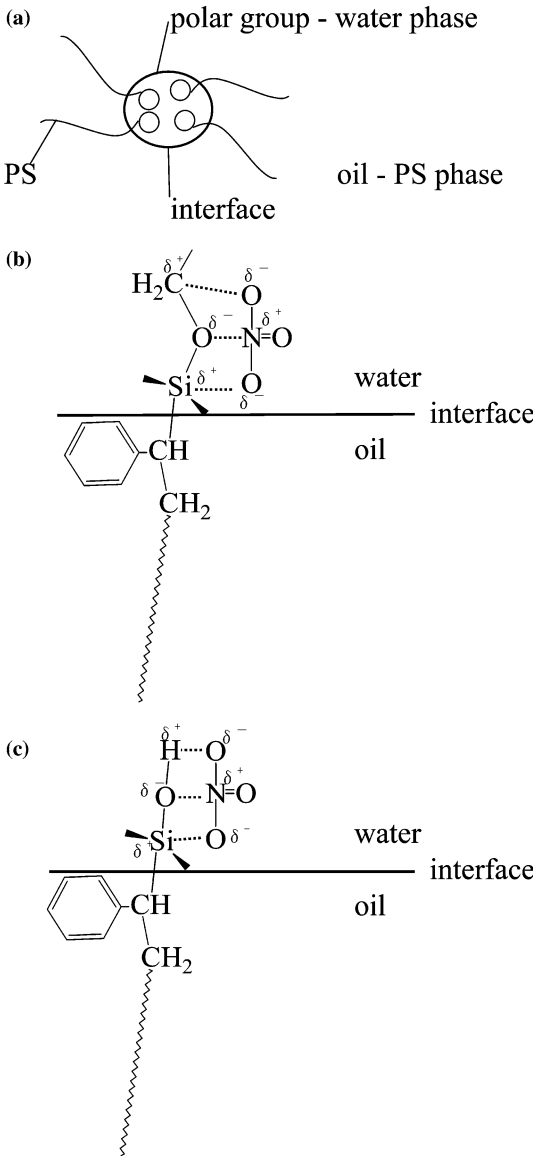

Fig. 5 Schematic structural models of the interface of a TESi-PS aggregate (**a**), and of the Si–O···NO_3 complexes ((**b**) and (**c**))

complex inhibits hydrolysis, and plays a critical role in production of dimers over a long time.

For the hydrolyzed and partially hydrolyzed monomeric species with SiOH groups, it is possible to form such complexes with the counter anion (Fig. 5c). The reactivity of an NO_3^--coordinated silanol is probably smaller than of an uncoordinated silanol, leading to slow progress of the polymerization.

The counter anions probably coordinate to the silanol or unreacted ethoxy groups of the trimeric and tetrameric molecules to form a oligomer-anions complex. Therefore, this coordination reduces the reactivity of these functional groups, hindering further growth of these oligomers.

Conclusion

The 2-D GPC correlation results of the HNO_3-catalyzed TESi-PS-THF-system may be summarized as follows.

1. Four monomeric species A, A_L, A_H and $A_{H'}$ appear predominantly in step I. These may be assigned to the solvated, unhydrolyzed monomer and to the mono-, di- and tri-hydrolyzed monomeric species, respectively. Furthermore, dynamic variation in population of the four monomeric components occurs to produce mainly the dimeric species (B_L and B) in step I.
2. Dynamic variation in population of component A occurs to predominantly form the B component, providing a very strong A ↔ B correlation in step II.
3. Although all four monomeric components exist in steps I and II, and react to produce dimeric and trimeric species, dynamic variation of component A is predominant in both steps.

From these results, we may assume that the four monomeric components (and in particular, component A) are relatively stable, resulting in reduction of the rate of polymerization. A hypothesis has been presented to explain this result.

References

1. Johannson OK, Stark FO, Vogel GE, Fleishmann RM (1967) J Compos Mater 1:278
2. Lee LH (1968) J Colloid Interface Sci 27:751
3. Schrader ME (1970) J Adhes 2:202
4. Bascom WD (1972) Macromolecules 5:792
5. Shih PTK, Koenig JL (1975) Mater Sci Eng 20:145
6. Batuev MI, Shostakovskii MF, Belyaev VI, Matvecva AD, Dubrova EW (1954) Dokl Akad Nauk SSSR 95:531
7. Batuev MI, Shostakovskii MF, Belyaev VI, Matvecva AD, Dubrova EW (1955) Chem Abstr 49:6089
8. Benesi HA, Jones AC (1959) J Phys Chem 63:179
9. Richards RE, Thompson HW (1949) J Chem Soc 124–132
10. Chiang CH, Ishida H, Koenig JL (1980) J Colloid Interface Sci 74:396
11. Murthy RSS, Leyden DE (1986) Anal Chem 58:1228
12. McKcnzie MT, Culler SR, Koenig JL (1984) Appl Spectrosc 38:786
13. Vranken KC, Van Der Voort P, Gillis-D'Hamers I, Vansant EF, Grobet P (1992) J Chem Soc Faraday Trans 88:3197
14. Shimizu I, Yoshino A, Okabayashi H, Nishio E, O'Connor CJ (1997) J Chem Soc Faraday Trans 93:1971

15. Shimizu I, Okabayashi H, Taga K, O'Connor CJ (1997) Colloid Polym Sci 275:555
16. Yoshino A, Okabayashi H, Shimizu I, O'Connor CJ (1997) Colloid Polym Sci 275:672
17. Okabayashi H, Shimizu I, Nishio E, O'Connor CJ (1997) Colloid Polym Sci 275:744
18. Shimizu I, Okabayashi H, Taga K, Nishio E, O'Connor CJ (1997) Vib Spectrosc 14:113
19. Shimizu I, Okabayashi H, Taga K, Yoshino K, Nishio E, O'Connor CJ (1997) Vib Spectrosc 14:125
20. Izawa K, Ogasawara T, Masuda H, Okabayashi H, Noda I (2002) Macromolecules 35:92
21. Izawa K, Ogasawara T, Masuda H, Okabayashi H, O'Connor CJ, Noda I (2002) J Phys Chem B 106:2867
22. Izawa K, Ogasawara T, Masuda H, Okabayashi H, O'Connor CJ, Noda I (2002) Phys Chem Chem Phys 4:1053
23. Suzuki K, Oku J, Izawa K, Okabayashi H, Noda I, O'Connor CJ (2004) Colloid Polym Sci (in press)
24. Suzuki K, Oku J, Izawa K, Okabayashi H, Noda I, O'Connor CJ (2004) Colloid Polym Sci (in press)
25. Suzuki K, Oku J, Izawa K, Okabayashi H, Noda I, O'Connor CJ (2004) J Polym Sci (in press)
26. Suzuki K, Katsumura G, Kondo Y, Oku J, Takaki M (1992) Koubunshi Ronbunshu 49:825
27. Noda I (1993) Appl Spectrosc 47:1329
28. Suzuki K, Oku J, Okabayashi H, O'Connor CJ (2003) Langmuir 19:7611
29. Takaki M, Suzuki K, Mano T (1991) Koubunshi Ronbunshu 48:171
30. Takaki M, Suzuki K, Kondo Y, Oku J (1991) Polym J 23:917